Fusion Engineering and Design 163 (2021) 112140

Contents lists available at ScienceDirect

Fusion Engineering and Design

journal homepage: www.elsevier.com/locate/fusengdes

RF discharge mirror cleaning for ITER optical diagnostics using 60 MHz very high frequency

L. Marot [a,*], L. Moser [a], R. Steiner [a], W. Erni [a], M. Steinacher [a], S. Dine [b], C. Porosnicu [c], C. P. Lungu [c], K. Soni [a], R. Antunes [a], F. Le Guern [d], J. Piqueras [d], E. Meyer [a]

[a] Department of Physics, University of Basel, Klingelbergstrasse 82, 4056 Basel, Switzerland
[b] SOLAYL SAS, 2 rue Jean Rostand, 91400 Orsay, France
[c] National Institute for Laser, Plasma and Radiation Physics, 409 Atomistilor Street, 077125 Magurele, Romania
[d] F4E, c/Josep Pla 2, Barcelona E-08019, Spain

ARTICLE INFO

Keywords:
ITER
First mirror
Plasma cleaning
End-of-Cleaning indicator

ABSTRACT

For the fusion reactor ITER, a mandatory monitor of the fusion device and plasma will be performed with optical diagnostic systems. For the metallic first mirrors, the recovery of the reflectivity losses due to dust deposition is proposed to be carried out for 14 different optical diagnostic systems by the plasma cleaning technique. In this work, we studied the influence of the electrode area on the electrode potential as a function of the applied power with a 60 MHz radio very high frequency source. Unshielded copper disks with different diameters were constructed to study the impact of the electrode area in the range of 90 cm^2 to 1200 cm^2, which corresponds to an Edge Thomson Scattering area ratio of 0.15 to 2. It was observed that the absolute value of the resulting bias decreased from 280 V to 15 V with the increase of the area for a given RF power. Moreover, the power consumption was reduced by 43 % using a pre-matching element close to the vacuum feedthrough. The cleaning homogeneity on a curved and a large size mirror was studied, and the difference between the center and edge maximum/minimum was around 20 % and 40 % for the curved and large size mirror, respectively. For ITER, it is required to have an End-of-Cleaning Indicator (ECI), which shows when the cleaning process would be stopped. In this work, we studied the feasibility of Optical Emission Spectroscopy (OES) as a real-time control tool for the RF cleaning process. With 13.56 or 60 MHz, it was possible to use OES as ECI by following the molybdenum (Mo), rhodium (Rh), and aluminum (Al) emission lines. The decrease of Al I line and increase of the Mo I and Rh I line were recorded as a function of the cleaning time.

1. Introduction

Metallic First Mirrors (FMs) will play a crucial role in numerous ITER optical diagnostic systems. Being the first element of the optical path, which allow radiation from the plasma to cross the neutron shielding, FMs will be subjected to erosion and/or deposition of first wall materials from fusion plasma. The net deposition can severely degrade the reflectivity of FMs, thus compromising the reliability of the optical measurements. For mirrors in net deposition conditions, plasma cleaning using radio-frequency (RF) discharges is currently being considered as the most promising in situ technique. This method was extensively reported in our recent paper [1,2] as well as the related questions [3]. Several research groups including Forschungszentrum Jülich, Germany [4]; Institute of Plasma Physics in Hefei, China [5]; Ioffe Institute in St. Petersburg, Russia [6]; TNO Delft, The Netherlands [7] are involved in finding solutions for mirror cleaning system. The review of the latest results is reported by Soni et al. [1].

In ITER, due to the considerable distance between the vacuum feedthrough and the FM, the distance between the RF generator and the FM will be in the order of few tens of meters [7,8]. The performance/optimization of the power transfer over a long distance and the coupling of RF with the mirror were investigated in this paper. Mostly for RF excitation, we considered in the manuscript 60 MHz as very high frequency (VHF), and only a few tests were carried out at 13.56 MHz high frequency (HF). The benefit of increasing the frequency is known; high ion fluxes are obtained at low ion energy even if power losses increase with frequency [9]. As the sheath thickness tends to decrease with increasing frequency, less collisions are expected at higher frequencies

* Corresponding author.
E-mail address: laurent.marot@unibas.ch (L. Marot).

https://doi.org/10.1016/j.fusengdes.2020.112140
Received 17 July 2020; Received in revised form 23 November 2020; Accepted 24 November 2020
Available online 11 December 2020

within the sheath [10]. It follows that the ion energy distribution is much more anisotropic. Moreover, VHF was predicted to be the most effective for Be cleaning with helium gas [11]. We also focused on several other aspects of the plasma cleaning technique integration for ITER diagnostic: evaluation/quantification of the uniformity of RF cleaning on flat and curved mirrors. The last section gives an insight into the End-of-Cleaning Indicator technique (ECI) using Optical Emission Spectroscopy (OES).

2. Experimental section

2.1. Setups and characterization techniques

The results presented in the manuscript were conducted using three different experimental facilities. Cleaning experiments and Optical Emission Spectroscopy (OES) measurements without beryllium (Be) were performed in a vacuum chamber with an internal grounded area of 9700 cm^2, which is referred as *chamber A* (Fig. 1a) hereafter [12]. The long cable experiment was carried out in a high vacuum chamber (Fig. 1d) with an area of 4800 cm^2 (*Chamber B*), using the electrode depicted in Fig. 1 of reference [2] and displayed in Fig. 1d) with an electrode area of 55.4 cm^2. OES tests with Be were realized in a controlled environment at the Beryllium Laboratory at the National Institute for Laser, Plasma and Radiation Physics (INFLPR, Romania) due to the toxicity of Be (especially in the form of dust) using *chamber C* (Fig. 1 of reference [13]). The argon pressure was first varied between 0.2–2 Pa to find the pressure that maximized the self-bias for a given power. The selected pressure was 0.2 Pa, which allowed to minimize the power density for a given ion energy.

For the OES measurements, a commercial spectrophotometer from Avantes was used (AvaSpec-2048-USB2-UA). This spectrophotometer can be used for UV/VIS/NIR, with a usable range of 200−1100 nm and a grating with 300 lines/mm. The focal length is 75 mm, and the resolution (FWHM) is 2.5 nm (slit size is 50 μm). The samples were analysed using Energy Dispersive X-ray Spectroscopy (EDX) for several electron energies (2−25 kV) using a SEM-FEI Nova Nano SEM230. The results were then fitted with the STRATAGem software [14] to estimate the amount of material (e.g., the thickness, if the density is known) in each layer according to the obtained X-ray counts and element properties. For the experiments requiring removal of contaminants for evaluation purposes, different types of thin films were deposited on mirror surfaces using magnetron sputtering, as described in reference [2,15]. Table 1 summarizes the mirror type, electrode's area, coating material, plasma frequency and technique used for the experiments carried out in the chambers A, B and C.

2.2. Radio-frequency feeding for 60 MHz

2.2.1. Components of the RF transmission

For the plasma cleaning experiments, the RF excitation frequency of 60 MHz (VHF) was supplied by a Comet generator (cito Plus 606-ACNA-N37A-FN) attached with a Comet matchbox (AGS 6020a MB). The connection from the matchbox to the vacuum feedthrough was implemented using a two-meter low-loss coaxial cable from Huber & Suhner S_10172_B-11. We used 7/16 DIN connectors for the RF power, allowing a maximum of 1.5 kW for 7.5 GHz RF (Fig. 1c). More details about the connector are given in reference [16]. The vacuum feedthrough for the long cable experiment was a coaxial feedthrough (Type N) mounted on a KF25 flange and it was followed by a coaxial copper RF feed with an inner diameter of 3 mm (Fig. 1d). More details about the vacuum

Table 1
Summary of the mirror type, electrode's area, coating material, plasma frequency and technique used for the experiments carried out in the chambers A, B and C.

Chamber	Mirror	Electrode area (cm^2)	Coating	Frequency (MHz)	Technique
Chamber A	ETS / Curved	90 to 1200 / 34	Rh / Mo / Al	60 / 13.56	Cleaning Test / OES
Chamber B		55		60	Pre-matching test / Long cable test
Chamber C	Flat small	10	Rh / Mo / Be	60	OES

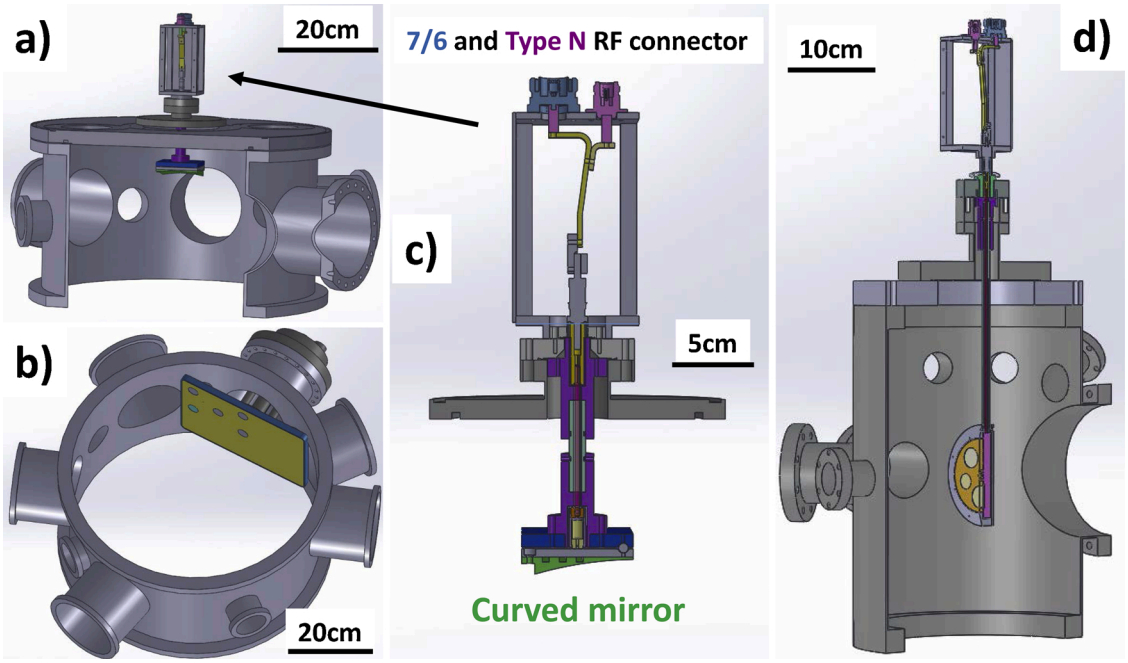

Fig. 1. a) Chamber A included the curved mirror; b) Chamber A with the ETS mock-up (top and bottom are not displayed): c) Zoom-in of the curved mirror electrode including the T connection with a 7/6 RF connector (blue) used for 2 and 10.6 m low-loss cable and a Type N RF connector (violet) used for 0.77 m low-loss cable or COMET vacuum capacitor which both are used as a pre-matching element; d) Section of chamber B.

feedthrough are in reference [17]. For the curved mirror, the vacuum feedthrough was a single pin feed (∅ = 3.9 mm) on a CF16 flange (Fig. 1c). More details about the vacuum feedthrough are presented in reference [18].

2.2.2. Pre-matching

Before the vacuum feedthrough was inserted, a pre-matching element of the type described by Leipold et al. [19] was mounted with a T connector of flat copper bars using a Type N connector (Fig. 1c). To reduce the power losses in the vacuum RF feed line, the pre-matching element should be located as close as possible to the mirror. Pre-matching elements can be capacitors or inductors inserted at the vacuum input to reduce the power reflection coefficient and therefore the power lost in the coaxial line between the matchbox and the vacuum chamber [7]. In our case, it was a 77 cm long open-ended coaxial transmission line connected in parallel at point "C" of reference [19] using a Type N RF connector (Fig. 1c). That cable was also the low-loss coaxial cable from Huber & Suhner (flexible cable model S_10172_B-11), which be replaced by an equivalent lumped component also connected in parallel. From the transmission line theory [20] the input impedance Z_{in} of that low-loss coaxial cable is equal to:

$$Z_{in} = Z_o\left(\frac{Z_{load} + jZ_0\tan(k \times L)}{Z_0 + jZ_{load}\tan(k \times L)}\right) \quad (1)$$

where Z_0 is the characteristic impedance of the cable (50 Ω), k the wave-number, L the line length (0.77 m), and Z_{load} the terminating impedance. Therefore, for an open-ended line ($Z_{load} \to +\infty$), the above formula becomes:

$$Z_{in} = -\frac{jZ_0}{\tan(k \times L)} \quad (2)$$

The electrical length is equal to:

$$k \times L = \frac{2\pi}{\lambda} \times L = \left(\frac{2\pi}{c \times VF}\right) \times f \times L \quad (3)$$

with f being the excitation frequency, VF the velocity factor and c the speed of light. The VF is equal to 87 % for the Huber & Suhner cable (insulator made of foamed polyethylene). With 60 MHz, the electrical length is therefore $k \times L = 1.11$ and $\lambda/2 = 2.17\ m$.

If the electrical length $k \times L$ is below $\pi/2$, then the imaginary part of Z_{in} is negative, and the equivalent component is a capacitor with an effective capacitance:

$$C_{eff} = \frac{\tan(k \times L)}{Z_0 \times 2\pi \times f} \quad (4)$$

The 77 cm long open-ended coaxial cable is therefore equivalent to a capacitor with $C_{eff} = 107$ pF.

The fixed open-ended coaxial cable was thus replaced by a vacuum variable vacuum capacitor (COMET CVBA-500AC/5-BFA-M) with an adjustable capacitance from 5 to 500 pF. A variable capacitor was found to be more compact and versatile than a fixed-length coaxial cable, albeit more expensive. A reduction of the power lost in the pre-matching system was also expected as vacuum capacitors have very low series resistances. The equivalent series resistance at 60 MHz is about 20 mΩ for the chosen vacuum capacitor, according to its manufacturer. Using the electrode presented in Fig. 1d) with Ar at 0.2 Pa and 60 MHz RF a negative self-bias of 280 V was obtained. As a convention, in the forthcoming sections of the manuscript, the negative self-bias displayed by the generator will be referred to its absolute value. Without pre-matching, an input power of 162 W was required. However, using the 77 cm long open-ended coaxial cable acting as pre-matching, only 98 W were needed as well as for the variable vacuum capacitor. In other words, for the experimental conditions mentioned above, 43 % less power was needed to achieve the same self-bias with pre-matching than without it. Moreover, no reduction of the power dissipated in the pre-matching system has been observed while using a vacuum capacitor instead of the open-ended coaxial cable.

2.2.3. Long RF cable

As mentioned in the introduction, in ITER the RF power generator and the matchbox will be installed far from the mirror [7]. Therefore, we replaced the two-meter cable with a 10.6 m long cable (initial length of 2 m plus 8.6 m corresponding to two RF wavelengths) and repeated the experiment using the same conditions mentioned above. The power loss in the long cables at 60 MHz was calculated as the function of cable length with the RF circuit analysis software SimSmith V14 [21], and results are plotted in Fig. 2 up to 20 m. The electrode impedance of reference [2] (Fig. 1d) was always used as the load impedance at the cable end ($Z_{load} = 4 - j26$ Ohms). The input impedance of the 77 cm open-ended coaxial cable calculated with SimSmith V14 is $Z = 0.078 - j24.6$ Ohms, which is the impedance of a 107 pF capacitor in series with a 78 mΩ resistor. As observed previously experimentally (section 2.2.2), the lost power is halved due to the pre-matching device regardless of the cable length. The dissipated power is the same irrespective of the pre-matching system: lossy 77 cm cable, lossy 107 pF capacitor and lossless 107 pF capacitor. The dissipated power in any pre-matching device is therefore negligible compared with the power lost in the cable between the matching network and the reactor input. The variable vacuum capacitor was found more convenient to use, but the significantly lower series resistance of the vacuum capacitor (20 mΩ) compared to the coaxial cable (78 mΩ) provided no visible improvement of the power coupling efficiency. This explains why a similar self-bias was measured in both cases for same input power. The input series resistance of the open-ended coaxial cable was already low enough to neglect the power loss inside.

3. Results and discussion

3.1. Power consumption for the first mirror: in-vessel tests

3.1.1. Measurements for large scale mirrors

As explained by Dmitriev et al. [22], the surface power density needed to obtain a given ion energy on the mirror is dependent on the excitation frequency, gas, and pressure, as well as the design of the mirror. For ITER, the goal is to reduce the power density for a given ion energy. In our case, the relation between the electrode's surface area and the RF power density on the ion energy (here the self-bias) was investigated using a ITER Edge Thomson Scattering mirror (ETS) (20 × 30

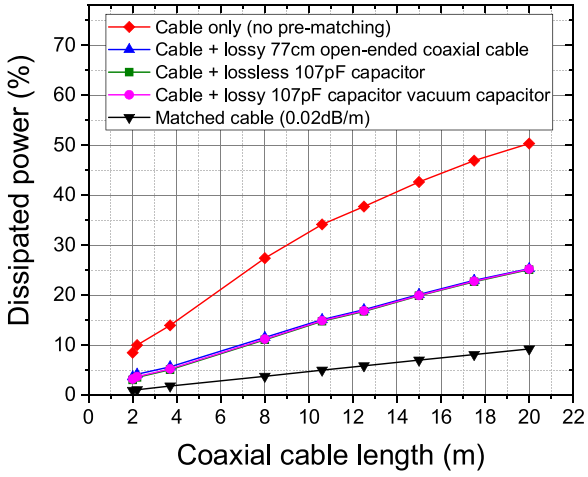

Fig. 2. Power loss in the cable and pre-matching device in percent of the input power as a function of the cable length without pre-matching element, using the 77 cm cable or capacitor, and with a matched cable. The magenta, green and blue curves overlap each other.

cm) (Fig. 4 of reference [23]) in *chamber A*. First of all, we observed that the shielding of the ETS-mirror was capacitively coupling some of the RF power and igniting a parasitic plasma when mounted like the curved mirror (Fig. 1a). The presence of this parasitic plasma dramatically lowered the self-bias on the working electrode. This phenomenon was never observed in our previous research work for HF with 13.56 MHz sources (Section 6.1 "Influence of size on the homogeneity" page 81 of Moser Ph.D. thesis [24]). By adding more ground loops to the shielding, it was possible to reduce parasitic plasmas with an improved shielding of the FM (Fig. 1b). Using a water cooled mirror and 60 MHz, 0.2 Pa, and Ar, a maximum of 140 V was achieved with the upper limit of the generator of 600 W (Fig. 3a). One possible explanation for the low self-bias is the broad area of the ETS mirror compared to the grounded area. However, the self-bias depends on the RF voltage (V_{rf}) as well as on the grounded area (A_g) and electrode area (A_e) [25]:

$$|V_{bias}| = V_{rf} \times \sin\left(\frac{\pi}{2} \times \frac{A_g - A_e}{A_g + A_e}\right) \tag{5}$$

For $A_g \gg A_e$, $|V_{bias}| \approx V_{rf}$ whereas for $A_g = A_e$, $|V_{bias}| = 0$. In our case $A_g = 9700$ cm^2 and $A_e = 600$ cm^2, hence $|V_{bias}| \approx 0.98 \times V_{rf}$. With this calculation, we can dismiss our previous argument and probably only attribute the low self-bias to the excitation frequency. Indeed, another experiment using 13.56 MHz excitation frequency was carried out, and 280 V was achieved at a lower power of 255 W; in comparison, only 86 V was obtained for the same power with 60 MHz. It is also known that increasing the driving voltage of a discharge increases the plasma density and ion current while maintaining the maximum ion energy (assuming the geometry, pressure, and voltage remain constant) [26]. Dmitriev et al. reported measurements for different gases and frequencies. As an example, for a constant power at 2 Pa, the neon mean ion energy decreased from 150 to 100 eV for 50 and 81 MHz, respectively

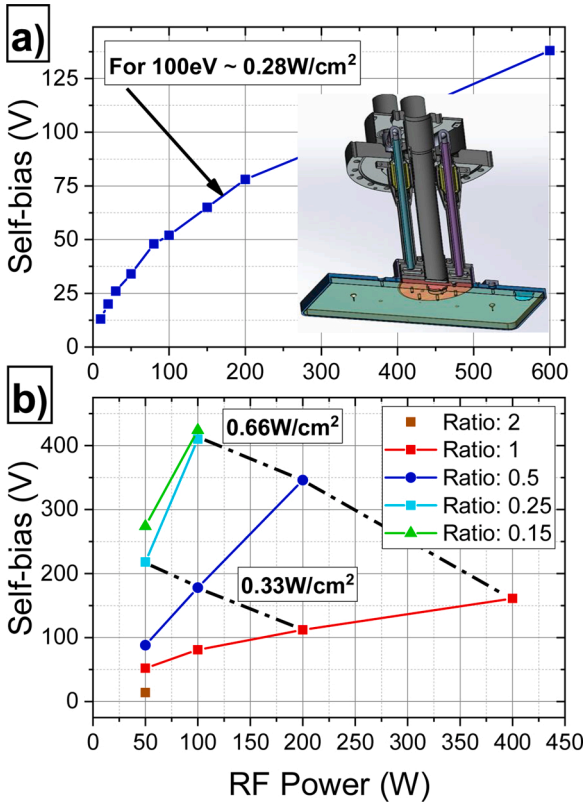

Fig. 3. a) Self-bias as a function of the RF power for the ETS mirror (area 600 cm^2). b) Self-bias as a function of the RF power for copper disks from 90 to 1200 cm^2, i.e., ETS area ratio from 0.15 to 2. Points connected by dashed lines have the same RF power density (0.33 or 0.66 W/cm^2).

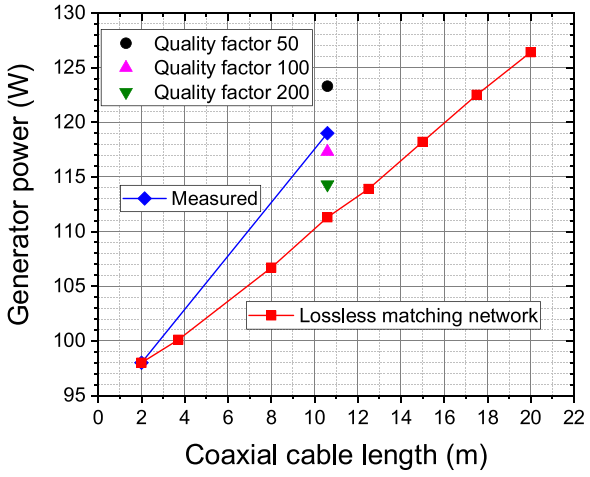

Fig. 4. Power needed to achieve 280 V self-bias as a function of the cable length using the chamber B and the electrode in Fig. 1d).

[22]. As seen in Fig. 3a) to achieve 100 eV (appropriate ion energy required for Be/BeO removal [22]), the surface power density is equal to 0.28 W/cm^2. The power density is defined as the ratio of the output generator power divided by the electrode size. Here we used 70 V self-bias, adding 30 V to the absolute value of the plasma potential. The plasma potential for this experiment was measured with a retarding field energy analyzer. In comparison, Dmitriev et al. [22] required 1 W/cm^2 at 81.36 MHz with neon gas at 1 Pa to achieve an equivalent ion energy.

3.1.2. *Discussion of the self-bias*

To further investigate the power consumption, unshielded copper disks with various areas (diameters) were constructed and mounted in the same position as the curved mirror (Fig. 1a) to study the impact of the electrode area in the range of 90 to 1200 cm^2, i.e., ETS area ratio from 0.15 to 2. We observe in Fig. 3b) that the resulting bias decreased from 280 to 15 V with the increase of the area ratio for a constant power of 50 W. This is in line with the accepted theory that as the powered electrode area increases in relation to the grounded area, the self-bias will decrease [27]. This is due to the decreasing flow of current to the ground that needs to be balanced. In Fig. 3b) is displayed in dashed line the self-bias achieved for the same power density (0.33 or 0.66 W/cm^2) and ETS area ratios of 1, 0.5, and 0.25. We have to keep in mind that $\sin\left(\frac{\pi}{2} \times \frac{A_g - A_e}{A_g + A_e}\right)$ vary from 0.94 to 0.99 for ETS area ratio from 0.15 to 2. Therefore, the change of asymmetry i.e., difference in areas A_g and A_e, can not explain the change in self-bias for constant surface power density.

To give an insight into these measurements, let's discuss more in detail the mechanism of RF power coupling in these discharges. The capacitive coupled plasma discharge can be treated as an electrical load, where the sheath behaves as a capacitor C_s in series with an inductor L_p due to electron inertia and resistor R_p because of electrons/ions' collisions in the plasma, respectively [28]. The bulk plasma inductance is usually negligible at high frequency (HF) like 13.56 MHz, and the bulk plasma impedance is equivalent to a simple resistor (in series with the sheath capacitance C_s).

According to the homogeneous sheath model for $\omega_{pi} \ll \omega \ll \omega_{pe}$ (ω, ω_{pi} and ω_{pe} the excitation, the ion and electron plasma frequency, respectively) [28], the voltage V_s across the sheath is related to the charge per unit area Q in the sheath by $V_s = Q^2/2e\varepsilon_0 n_0$ such that the sheath capacitance per unit electrode area (ε_0 is the vacuum permittivity and n_0 is the plasma density assumed homogeneous),

$$C_s = \frac{Q}{V_s} = \left(\frac{2e\varepsilon_0 n_0}{V_s}\right)^{1/2} \tag{6}$$

depends inversely on the square root of the voltage V_s. There is a discharge series resonance when $\omega_{res} = 1/\sqrt{C_s L_p}$, which enhances the RF current at constant RF voltage. As previously described, with the assumption that $\omega \ll \omega_{pe}$, the bulk plasma with effective length l_p can be characterized by an inductance per unit (electrode) area of $L_p = l_p/\varepsilon_0\omega_p^2$ and a resistance per unit area $R_p = \nu_m L_p$ (ν_m is the electron-neutral momentum transfer frequency, which is proportional to the gas pressure and $\omega_{pe}^2 = e^2 n_e/\varepsilon_0 m$ is the square of the electron plasma frequency) [29,30]. The sheath capacitance per unit electrode area is $C_s = \varepsilon_0/s$. The discharge series resonance frequency is therefore equal to $\omega_{res} = 1/\sqrt{C_s L_p} = \omega_{pe}\sqrt{s/l_p}$ where s is the sheath width.

In most conventional RF discharges the resonance frequency has been experimentally reported by Godyak and Popov for VHF ($\geq$ 40 MHz) and with really low V_{bias} until 5 V [31,32]. Moreover, Qui et al. [33], reported for 81.36 MHz with Ar at 0.4 Pa that the minimum RF voltage amplitude to sustain the discharge was only of the order of the electron temperature (i.e, a few volts) and occurred when the RF current and RF voltage were in phase. Our experimental conditions are quite close to those of Qui et al. [33], and we explained the low V_{bias} near the ω_{res}. Moreover, L_p is proportional to the bulk resistance and it decreases when the power increases. Therefore, the resonance condition is always observed at low power. Furthermore, increasing the area ratio leads to an increase of C_s and a decrease of V_s in Eq. (6) i.e. a decrease of V_{bias}.

Moreover, it should be noted that Eq. (5) is valid at low frequencies for $\omega \leq \omega_{pi}$, where $\omega_{pi} = \left(e^2 n_i/\varepsilon_0 M\right)^{1/2}$ is the ion plasma frequency at the sheath edge [34]. For VHF like 60 MHz, most probably, this is not anymore the case and the electrical circuit equivalent to the plasma is therefore distributed as inductance and capacitance [30]. We can express $|V_{bias}|$ as reported by Raizer et al., [35] when the sheath behave as a constant capacitor:

$$|V_{bias}| = V_{rf}\left(\frac{C_e - C_g}{C_e + C_g}\right) \tag{7}$$

where C_e and C_g are the capacitances of the sheaths at the excitation electrode and the grounded electrode, respectively. C_e and C_g are calculated with

$$C_e = \frac{\varepsilon_0 A_e}{s_e} \; ; \; C_g = \frac{\varepsilon_0 A_g}{s_g} \tag{8}$$

where s_e and s_g are, respectively, the sheath thickness in front of the driven electrode and the wall (ground). Thus, we can deduce in a similar way that with increasing area ratio, C_e increases and $|V_{bias}|$ decreases.

3.2. Power consumption for the first mirror: ex-vessel test

As mentioned in the introduction, in order to perform/optimize the power transfer on a long distance and the coupling of RF on the mirror, tests were performed ex-vessel. Using the electrode depicted in Fig. 1 of reference [2] in the vacuum *chamber B* (Fig. 1d) and Ar gas at 0.2 Pa with 60 MHz for 280 V self-bias with the two-meter long cable, 98 W was required. With 10.6 m long cable, 119 W was needed, i.e., 21 W of additional power. Generator power calculations were carried out with SimSmith V14 as a function of the coaxial cable length (between the matching network and the pre-matching device) to keep the power at the reactor input the same (94.4 W) and to ensure the same self-bias. The results are shown in Fig. 4 when the matching network is assumed lossless (red curve). The calculated power with a 10.6 m long cable is 111 W, which is only 8 W below the experimental value (blue curve). The lost power in the matching network could reasonably explain the 8 W difference. The latter is a L-type matching network with a fixed inductor (130 nH) in series with the output. That inductor is commonly labeled the "tune" in the literature. The other components in the matching circuit are vacuum capacitors. The primary sources of power dissipation within a matching network are usually the inductors. Their quality factors Q are generally in the range of 30–300, much lower than the quality factors of the vacuum capacitors (typically about 1000). The generator power was also calculated for a lossy matching network for a cable length of 10.6 m, assuming a quality factor for the tuning inductor between 50 and 200, in other words, a series resistance between 0.25 and 1 Ω at 60 MHz. The results confirm that the lost power in the matching network could reasonably explain the 8 W difference.

3.3. Demonstration of the cleaning efficiency and homogeneity

Following the optimization stage, the main idea was to evaluate/quantify the uniformity of RF cleaning on flat and curved mirrors. For this purpose, two experiments were performed using the same procedure, with (i) a curved mirror with 8.4 × 4 cm and a curvature of R = 12 cm and (ii) the ETS mock-up mirror in the *chamber A*. The former curved mirror was part of a first mirror unit mock-up (half size) of the Hα diagnostics [36]. To measure the erosion homogeneity, the curved mirror was coated with a 400 nm thick rhodium film. Tests were carried out in *chamber A* (Fig. 1a), and the cleaning parameters were 45 W RF generator output power, 60 MHz, 0.2 Pa using Ar gas with 300 eV of ion energy (which is equivalent to 0.9 W/cm^2). The uniformity of the cleaning was evaluated by EDX measurements (before and after) at various locations. The EDX measurements point 1, 2, 3, and 6 are close to 2.5 cm from the center M (Fig. 5a). The curvature has a slight effect on the sputtering rate (Fig. 5a). The inhomogeneity, defined as maximum/minimum = (max-min)/min (%), was around 20 % after 85 min. After one further cleaning cycle, we can observe edge effects (faster cleaning on edge). From our previous study, edge effects mostly impact the first few centimeters of the mirror [24].

As mentioned, the objective and procedure for the water-cooled ETS mirror shown in Fig. 1b were the same. The plasma parameters were 600 W RF generator output power, 60 MHz, 0.2 Pa Ar gas with 130 eV ion energy (which corresponds to 1 W/cm^2). To measure the erosion homogeneity, the insets of the ETS mirror were coated with a 400 nm thick molybdenum film. After 130 min, the inhomogeneity between the center and edge maximum/minimum was ≈ 40 %. As displayed in Fig. 5b), two kinds of sputtering regimes were observed. A low sputtering rate for positions 1 and 2 and a higher rate for the three other locations.

3.4. Proof of concept for the End-of-Cleaning Indicator

In order to spare the mirror surface, i.e. its reflective coating or the polished bulk material from damage due to exaggerated cleaning, an ECI is necessary to stop the cleaning process timely. One possible method consists of measuring the reflectance of the mirror in situ by using a light source in the plasma of the cleaning discharge. The idea is to use a singular light source present in the discharge, namely fast atoms of hydrogen, and determine the ratio of the light emitted in the direction of the observer to the light received after reflection on the mirror surface [37]. Another possible technique for the ECI could be OES as a real-time control tool for the RF cleaning process [38]. To experiment with another solution for ITER, OES was selected for this work. The characteristic emission lines used for the proof of concept for the ECI are presented in Table 2 [39,40].

OES measurements were carried out in the *chamber C* during the plasma cleaning of a Be deposit film. In the case of plasma cleaning of the Be film using 60 MHz and 200 V self-bias with Ar, He and D_2 at 1.4 Pa, no Be emission lines were observed. To be able to visualize Be lines, we decided to perform OES on a more dense and confined plasma, i.e., in front of a Be magnetron target [13]. Be I ground state emission lines were observed with the magnetron in DC or RF mode (Fig. 6), although Be II ground state emission line at 527.1 nm was not detected. This is due to the higher ionization energy, 18.2 instead of 9.32 eV for BII and BeI, respectively. A similar situation was obtained for Mo and Rh films. At lower wavelengths (< 300 nm), emission lines were registered from Be

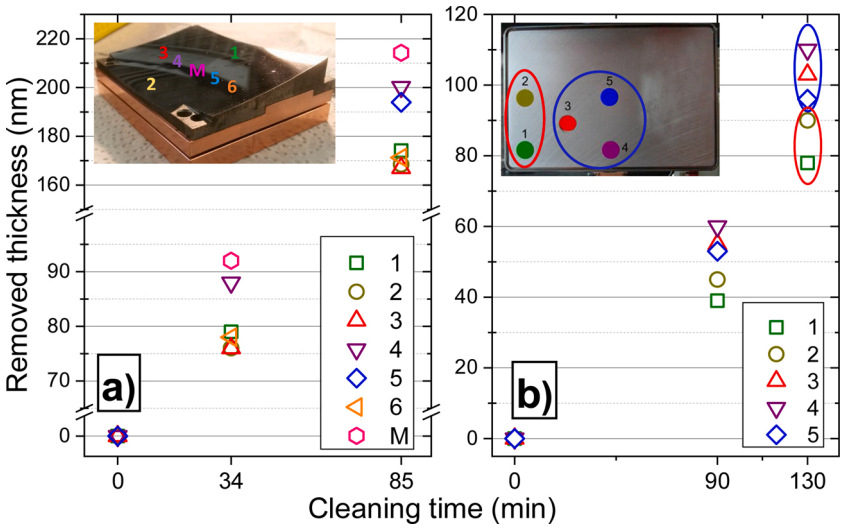

Fig. 5. a) Removed thickness of Rh a) and Mo b) as function the cleaning time for the curved and ETS mirror.

Table 2
Transition and corresponding wavelength for Al, W, Be, Mo, and Rh ground state. Data from references [39,40].

Spectrum / Ionization energy (eV)	Configuration	Wavelength (nm)
Al I / 5.99	$3s^2(^1S)3p\text{-}3s^2(^1S)4s$	394.40
Al I / 5.99	$3s^2(^1S)3p\text{-}3s^2(^1S)4s$	396.15
Al I / 5.99	$3s^2(^1S)3p\text{-}3s^2(^1S)3d$	308.22
Al I / 5.99	$3s^2(^1S)3p\text{-}3s^2(^1S)3d$	309.27
W I / 7.86	$5d^5(^6S)6s\text{-}5d^5(^6S)6p$	400.88
Be I / 9.32	2s2p-2s3s	332.13
Be I / 9.32	2s2p-2s3d	457.27
Be I /9.32	$2s^2\text{-}2s2p$	234.86
Be II / 18.2	$1s^23p\text{-}1s^24s$	527.03
Mo I / 7.01	$4d^5(^6S)5s\text{-}4d^5(^6S)5p$	379.83
Mo I / 7.01	$4d^5(^6S)5s\text{-}4d^4(^5D)5s(^6D)5p$	313.26
Rh I / 7.46	$4d^8(^3F)5s\text{-}4d^8(^3F)5p$	369.24

and Rh but not Mo, as depicted in Fig. 6b). In summary, ECI was unsuccessful during plasma cleaning of Be deposits, but it performed well during Be magnetron sputtering.

To further investigate the ECI technique, it was decided to perform experiments with aluminum used as Be surrogate [41] in *chamber A* at the University of Basel. Using 13.56 or 60 MHz, it was possible to use OES as ECI by following the molybdenum, rhodium, and aluminum emission lines. As for the previous Be measurements, using plasma cleaning parameters of Ar gas at 0.2 Pa, 280 V self-bias, no emission lines of Al were recorded. Since the ionization of the sputtered particles typically depends on the working pressure, we overcame this issue by increasing the pressure to 2 Pa. The power was kept constant which resulted in a decrease of the self-bias to 140 V. With these conditions, Fig. 7a) shows Al and Rh signal, while Fig. 7c) shows Al and Mo emission lines. Experiments were done on the curved mirror (Rh coated) employed for the cleaning campaign in section 3.2 and reused here for the ECI tests with Al contamination (approximatively 50 nm). As the thin Al layer is sputtered away from the surface as a result of the physical sputtering, the signal of the Al emission lines should decrease. In contrast, the intensity for the Rh emission lines, which is the optical mirror coating, should increase. For t<0 min (Fig. 7b), the reference point is the OES intensity of the Rh mirror before Al coating. When the cleaning starts (t>0 min), the Al lines decrease while the Rh lines increase, indicating the removal of Al.

In the case of Mo mirror, experiments were performed with 20 nm Al contamination and the cleaning realized with an excitation of 13.56 MHz and Ar gas at 3 Pa for 14 min with 400 V self-bias (Fig. 7c). When

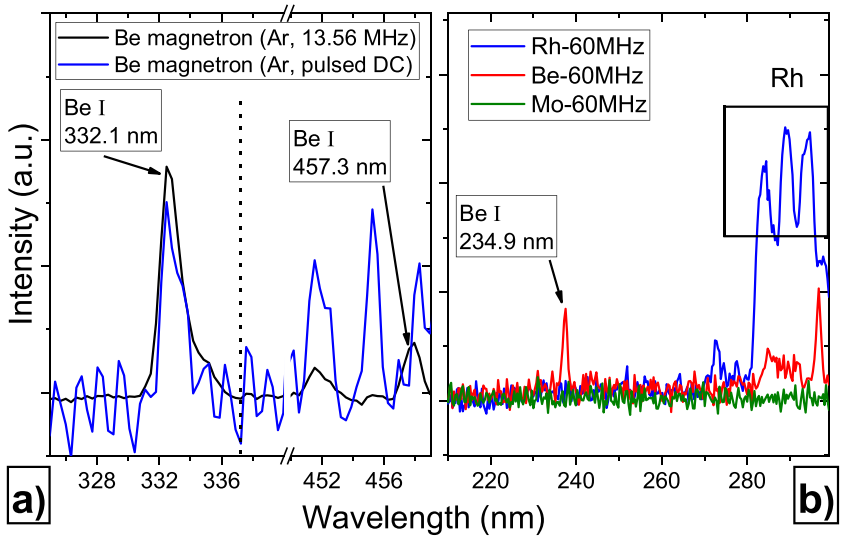

Fig. 6. a) OES of magnetron sputtering using a Be target with DC and RF excitation. b) OES during plasma cleaning using 60 MHz excitation.

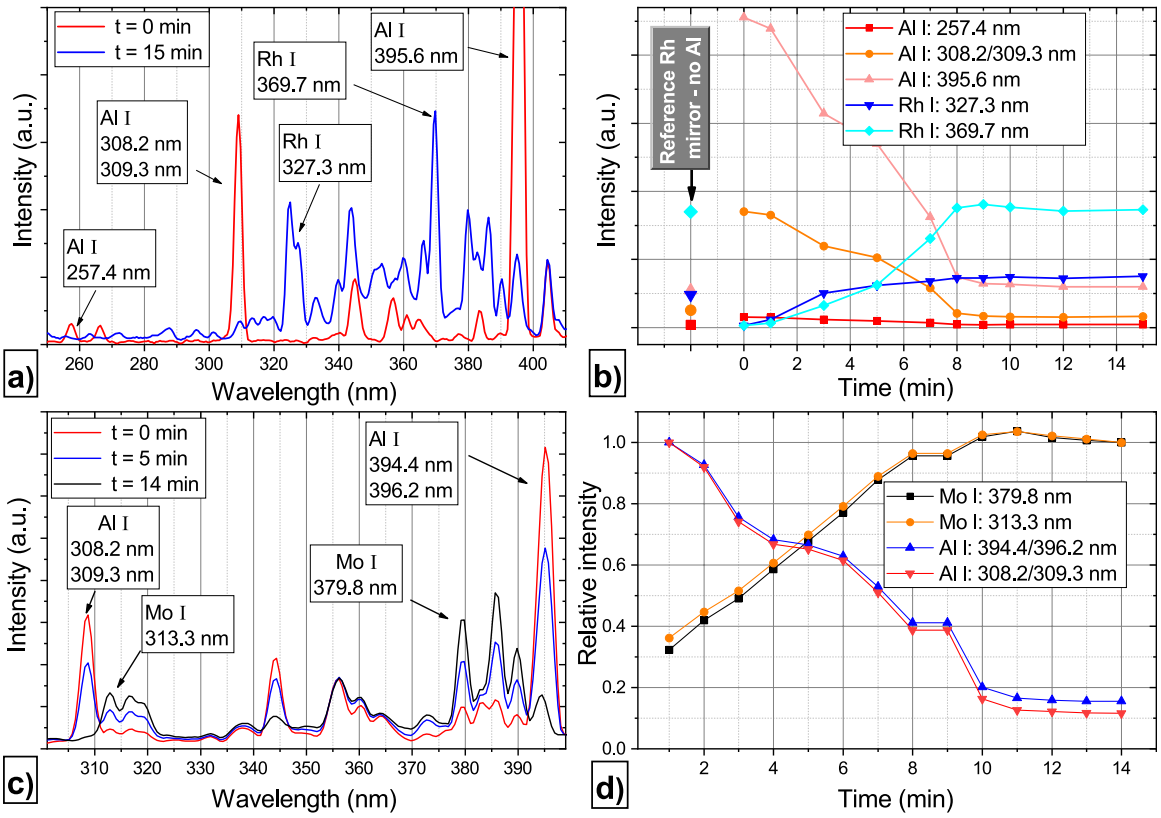

Fig. 7. OES measurements obtained with a) Rh and c) Mo mirrors contaminated with Al, using 60 and 13.56 MHz Ar plasma. The ECI is shown in b) and d) for Rh and Mo, respectively.

the cleaning starts (t > 0 min), the Al lines decrease while the Mo lines increase, indicating the removal of Al (Fig. 7d). To summarize, ECI was successfully demonstrated using the OES technique for Al deposits on Rh and Mo mirrors.

During the mirror cleaning campaigns in ITER, we foresee running the cleaning plasma at low pressures (0.2 Pa) and periodically increase the pressure (2 Pa) to detect the emission lines of Be, to follow the cleaning progress.

4. Conclusion

Since the surface power density requested to reach a sufficiently high ion energy is dependent on several parameters, the relation between the electrode surface and the RF power density was investigated using a ITER Edge Thomson Scattering mirror (600 cm^2) with unshielded Cu disks with various areas (diameters), comprising an ETS area ratio from 0.15 to 2. It was observed that the resulting bias decreased from 280 V to 15 V with the increase of the area for a given RF power. In addition, the power consumption was reduced by 43 % using a pre-matching element close to the vacuum feedthrough. The cleaning homogeneity on a curved and large size mirror was studied, and the difference between the center and edge maximum/minimum was found to be around 20 and 40 %, respectively. Moreover, plasma cleaning with OES as ECI was successfully performed for 60 MHz with Rh or Mo mirrors and a Al film deposited on top. For the 13.56 MHz excitation, the End-of-Cleaning Indicator during plasma cleaning is also effective with a Mo mirror and a Al film. One possible criteria for stopping the plasma cleaning using OES as ECI is to get the same intensity of the emission line of interest as for the pristine mirror.

CRediT authorship contribution statement

L. Marot: Writing - original draft, Supervision, Project administration, Funding acquisition. **L. Moser:** Investigation, Visualization, Writing - review & editing. **R. Steiner:** Methodology, Investigation. **W. Erni:** Resources. **M. Steinacher:** Resources. **S. Dine:** Methodology, Resources, Formal analysis, Visualization, Writing - review & editing. **C. Porosnicu:** Resources. **C.P. Lungu:** Resources. **K. Soni:** Investigation. **R. Antunes:** Writing - review & editing. **F. Le Guern:** Conceptualization, Project administration. **J. Piqueras:** Conceptualization, Project administration. **E. Meyer:** Project administration.

Declaration of Competing Interest

The authors declare that they have no known competing financial interests or personal relationships that could have appeared to influence the work reported in this paper.

Acknowledgments

The authors would like to thank the Swiss Federal Office of Energy, Swiss Nanoscience Institute, Swiss National Science Foundation and the Federal Office for Education and Science are acknowledged for their financial support. The work leading to this publication has been funded partially by Fusion for Energy under contract F4E-OPE-0851. This publication reflects the views only of the author, and Fusion for Energy cannot be held responsible for any use which may be made of the information contained therein. We thank Dr. Andrey Alekseev for giving us the first mirror unit mock-up of the Hα diagnostics.

References

[1] K. Soni, L. Moser, R. Steiner, D. Mathys, F. Le Guern, J. Piqueras, L. Marot, E. Meyer, Plasma cleaning of steam ingressed ITER first mirrors, Nucl. Mater. Energy 21 (2019) 100702, https://doi.org/10.1016/j.nme.2019.100702.

[2] L. Moser, L. Marot, R. Steiner, R. Reichle, F. Leipold, C. Vorpahl, F. Le Guern, U. Walach, S. Alberti, I. Furno, R. Yan, J. Peng, M. Ben Yaala, E. Meyer, Plasma cleaning of ITER first mirrors, Phys. Scr. T170 (2017), 014047, https://doi.org/10.1088/1402-4896/aa8f30.

[3] A. Litnovsky, V.S. Voitsenya, R. Reichle, M. Walsh, A. Razdobarin, A. Dmitriev, N. Babinov, L. Marot, L. Moser, R. Yan, M. Rubel, A. Widdowson, S. Moon, S.G. Oh, Y. An, P. Shigin, I. Orlovskiy, K.Yu. Vukolov, E. Andreenko, A. Krimmer, V. Kotov, Ph. Mertens, Specialists working group on first mirrors of the ITPA topical group on diagnostics, diagnostic mirrors for ITER: research in the frame of international tokamak physics activity, Nucl. Fusion 59 (2019), 066029, https://doi.org/10.1088/1741-4326/ab1446.

[4] J. Peng, A. Litnovsky, A. Kreter, Yu. Krasikov, M. Rasinski, U. Breuer, J.L. Chen, Sputtering tests of single crystal molybdenum and rhodium mirrors at high ion fluence for in situ plasma cleaning of first mirrors in ITER, Fusion Eng. Des. 128 (2018) 107–112, https://doi.org/10.1016/j.fusengdes.2018.01.061.

[5] R. Yan, L. Moser, B. Wang, J. Peng, C. Vorpahl, F. Leipold, R. Reichle, R. Ding, J. Chen, L. Mu, R. Steiner, E. Meyer, M. Zhao, J. Wu, L. Marot, Plasma cleaning of ITER edge Thomson scattering mock-up mirror in the EAST tokamak, Nucl. Fusion 58 (2018), 026008, https://doi.org/10.1088/1741-4326/aa96b8.

[6] A.M. Dmitriev, N.A. Babinov, A.N. Bazhenov, I.M. Bukreev, D.I. Elets, V. V. Filimonov, A.N. Koval, G.S. Kueskiev, A.E. Litvinov, E.E. Mikhin, A. G. Razdobarin, D.S. Samsonov, V.A. Senitchenkov, V.A. Solovei, I.B. Terechenko, S. Yu. Tolstyakov, L.A. Varshavchik, P.V. Chernakov, Al.P. Chernakov, An. P. Chernakov, S.N. Tugarionov, P.A. Shigin, F. Leipold, R. Reichle, M. Walsh, A. Pflug, RF plasma cleaning of water-cooled mirror equipped with notch filter based on shorted λ/4 line, Fusion Eng. Des. 146 (2019) 1390–1393, https://doi.org/10.1016/j.fusengdes.2019.02.090.

[7] A. Ushakov, A. Verlaan, U. Stephan, O. Steinke, M. de Bock, M.P. Maniscalco, P. Verhoeff, ITER visible spectroscopy reference system first mirror plasma cleaning in radio-frequency gas discharge – circuit design and plasma effects, Fusion Eng. Des. 154 (2020) 111546, https://doi.org/10.1016/j.fusengdes.2020.111546.

[8] M. Walsh, P. Andrew, R. Barnsley, L. Bertalot, R. Boivin, D. Bora, R. Bouhamou, S. Ciattaglia, A.E. Costley, G. Counsell, M.F. Direz, J.M. Drevon, A. Encheva, T. Fang, M. von Hellermann, D. Johnson, J. Kim, Y. Kusama, H.G. Lee, B. Levesy, A. Martin, P. Maquet, K. Okayama, R. Reichle, K. Patel, C.S. Pitcher, A. Prakash, S. Simrock, N. Taylor, V.S. Udintsev, Y. Utin, P. Vasu, G. Vayakis, E. Veshchev, B. Schunke, C. Walker, C. Watts, A. Zvonkov, ITER Diagnostic Challenges, IEEE, 2011, pp. 1–8, https://doi.org/10.1109/SOFE.2011.6052210.

[9] A. Perret, P. Chabert, J. Jolly, J.-P. Booth, Ion energy uniformity in high-frequency capacitive discharges, Appl. Phys. Lett. 86 (2005), 021501, https://doi.org/10.1063/1.1848183.

[10] M. Surendra, D.B. Graves, Capacitively coupled glow discharges at frequencies above 13.56 MHz, Appl. Phys. Lett. 59 (1991) 2091–2093, https://doi.org/10.1063/1.106112.

[11] A.M. Dmitriev, N.A. Babinov, A.N. Bazhenov, I.M. Bukreev, M.M. Kochergin, A. N. Koval, G.S. Kurskiev, A.E. Litvinov, S.V. Masyukevich, E.E. Mukhin, A. G. Razdobarin, D.S. Samsonov, V.V. Solokha, S.Y. Tolstyakov, P. Andrew, F. Leipold, P.A. Shigin, R. Reichle, V.L. Bukhovets, A.E. Gorodetsky, A.V. Markin, A.P. Zakharov, R.K. Zalavutdinov, A.P. Chernakov, A.P. Chernakov, P. V. Chernakov, T.V. Chernoizumskaya, A.A. Kobelev, A.S. Smirnov, I. A. Marzinovsky, *In situ* plasma cleaning of ITER diagnostic mirrors in noble-gas RF discharge, Phys. Scr. T170 (2017), 014072, https://doi.org/10.1088/1402-4896/aa95e5.

[12] S. Iyyakkunnel, L. Marot, B. Eren, R. Steiner, L. Moser, D. Mathys, M. Düggelin, P. Chapon, E. Meyer, Morphological changes of tungsten surfaces by low-flux helium plasma treatment and helium incorporation via magnetron sputtering, ACS Appl. Mater. Interfaces 6 (2014) 11609–11616, https://doi.org/10.1021/am502370t.

[13] M. Ben Yaala, L. Moser, R. Steiner, B. Butoi, P. Dinca, P. Petersson, L. Marot, E. Meyer, Deuterium as a cleaning gas for ITER first mirrors: experimental study on beryllium deposits from laboratory and JET-ILW, Nucl. Fusion 59 (2019), 096027, https://doi.org/10.1088/1741-4326/ab2d31.

[14] F. Galbert, Measurement of carbon layer thickness with EPMA and the thin film analysis software STRATAGem, Microsc. Microanal. 13 (2007), https://doi.org/10.1017/S1431927607080488.

[15] B. Eren, L. Marot, M. Wisse, D. Mathys, M. Joanny, J.-M. Travère, R. Steiner, E. Meyer, In situ evaluation of the reflectivity of molybdenum and rhodium coatings in an ITER-like mixed environment, J. Nucl. Mater. 438 (2013) S852–S855, https://doi.org/10.1016/j.jnucmat.2013.01.184.

[16] M. Hannon, P. Malloy, Application Guide to RF Coaxial Connectors and Cables, 2014. https://www.arworld.us/pdfs/appNotes/AppNote51b.pdf.

[17] Type N-feedthrough on flange KF25, (n.d.). http://www.vacom-shop.de/epages/VacomShop.sf/en_GB/?ObjectPath=/Shops/Store.VacomShop/Products/301801.

[18] Single pin feedthrough on flange CF16, (n.d.). http://www.vacom-shop.de/epages/VacomShop.sf/en_GB/?ViewObjectID=1716435.

[19] F. Leipold, R. Reichle, C. Vorpahl, E.E. Mukhin, A.M. Dmitriev, A.G. Razdobarin, D. S. Samsonov, L. Marot, L. Moser, R. Steiner, E. Meyer, Cleaning of first mirrors in ITER by means of radio frequency discharges, Rev. Sci. Instrum. 87 (2016), 11D439, https://doi.org/10.1063/1.4962055.

[20] S. Ramo, J. Whinnery, T. Van Duzer, Fields and Waves in Communication Electronics, 1994. ISBN: 978-0-471-58551-0.

[21] N.d. http://www.ae6ty.com/Smith_Charts.html.

[22] A.M. Dmitriev, N.A. Babinov, A.N. Bazhenov, I.M. Bukreev, D.I. Elets, V. V. Filimonov, A.N. Koval, G.S. Kueskiev, A.E. Litvinov, E.E. Mikhin, A. G. Razdobarin, D.S. Samsonov, V.A. Senitchenkov, V.A. Solovei, I.B. Terechenko, S. Yu. Tolstyakov, L.A. Varshavchik, P.V. Chernakov, Al.P. Chernakov, An. P. Chernakov, S.N. Tugarionov, P.A. Shigin, F. Leipold, R. Reichle, M. Walsh, A. Pflug, RF plasma cleaning of water-cooled mirror equipped with notch filter based on shorted λ/4 line, Fusion Eng. Des. 146 (2019) 1390–1393, https://doi.org/10.1016/j.fusengdes.2019.02.090.

[23] L. Moser, R. Steiner, F. Leipold, R. Reichle, L. Marot, E. Meyer, Plasma cleaning of ITER First Mirrors in magnetic field, J. Nucl. Mater. 463 (2015) 940–943, https://doi.org/10.1016/j.jnucmat.2014.11.087.

[24] Lucas Moser, Plasma Cleaning of Diagnostic First Mirrors for the Nuclear Fusion Machine ITER, PhD Thesis, University of Basel, 2017, http://edoc.unibas.ch/56229/1/Thesis_LucasMoser.pdf.

[25] E. Kawamura, V. Vahedi, M.A. Lieberman, C.K. Birdsall, Ion energy distributions in rf sheaths; review, analysis and simulation, Plasma Sources Sci. Technol. 8 (1999) R45–R64, https://doi.org/10.1088/0963-0252/8/3/202.

[26] M. Surendra, D.B. Graves, Capacitively coupled glow discharges at frequencies above 13.56 MHz, Appl. Phys. Lett. 59 (1991) 2091–2093, https://doi.org/10.1063/1.106112.

[27] D. Shaw, E. Wagenaars, Modelling radio-frequency plasma cleaning of fusion optics, Plasma Phys. Control. Fusion. 61 (2019), 085031, https://doi.org/10.1088/1361-6587/ab2cb2.

[28] M.A. Lieberman, A.J. Lichtenberg, E. Kawamura, T. Mussenbrock, R.P. Brinkmann, The effects of nonlinear series resonance on Ohmic and stochastic heating in capacitive discharges, Phys. Plasmas 15 (2008), 063505, https://doi.org/10.1063/1.2928847.

[29] A.A. Howling, L. Sansonnens, J. Ballutaud, Ch. Hollenstein, J.P.M. Schmitt, Nonuniform radio-frequency plasma potential due to edge asymmetry in large-area radio-frequency reactors, J. Appl. Phys. 96 (2004) 5429–5440, https://doi.org/10.1063/1.1803608.

[30] P. Chabert, N. Braithwaite, Physics of Radio-frequency Plasmas, Cambridge University Press, Cambridge, 2011.

[31] V.A. Godyak, O.A. Popov, Experimental study of resonant RF discharges, Sov. J. Plasma Phys. 5 (1979) 227–231.

[32] V.A. Godyak, Soviet Radio Frequency Discharge Research, Delphic Associates, 1986.

[33] W.D. Qiu, K.J. Bowers, C.K. Birdsall, Electron series resonant discharges: comparison between simulation and experiment, Plasma Sources Sci. Technol. 12 (2003) 57–68, https://doi.org/10.1088/0963-0252/12/1/308.

[34] M.A. Lieberman, A.J. Lichtenberg, Principles of Plasma Discharges and Materials Processing: Lieberman/Plasma 2e, John Wiley & Sons, Inc., Hoboken, NJ, USA, 2005, https://doi.org/10.1002/0471724254.

[35] Y.P. Raizer, M.N. Shneider, N.A. Yatsenko, Radio-Frequency Capacitive Discharges, 1st ed., CRC Press, 2017 https://doi.org/10.1201/9780203741337.

[36] I. Orlovskiy, E. Andreenko, A. Alekseev, Estimation of neutral fluxes on the first mirror of H-alpha diagnostics in ITER, Fusion Eng. Des. 146 (2019) 827–830, https://doi.org/10.1016/j.fusengdes.2019.01.091.

[37] P. Mertens, The core-plasma CXRS diagnostic for ITER: an introduction to the current design, J. Fusion Energy. 38 (2019) 264–282, https://doi.org/10.1007/s10894-018-0202-1.

[38] Yu.V. Kapustin, A.V. Rogov, D.K. Vukolov, A.V. Gorbunov, The Integration of DC/PDC Cleaning System Electrodes Into H-alpha Diagnostic First Mirror Unit, Novosibirsk, Russia, 2016. https://sharepoint.iter.org/departments/POP/ITPA/Diag/DIAG/_layouts/15/WopiFrame.aspx?sourcedoc=%7B6FA5DD68-9F6A-404E-9331-3F5192ABF157%7D&file=09.Kapustin.Integration.DC.PDC.plasma.cleaning.systems.into.H-alpha.diagnostic.pptx&action=default&CT=1607364857741&OR=DocLibClassicUI.

[39] J.E. Sansonetti, W.C. Martin, Handbook of basic atomic spectroscopic data, J. Phys. Chem. Ref. Data 34 (2005) 1559–2259, https://doi.org/10.1063/1.1800011.

[40] A. Kramida, Y. Ralchenko, J. Reader, NIST ASD Team, NIST Atomic Spectra Database, 2019, https://doi.org/10.18434/T4W30F.

[41] L. Marot, C. Linsmeier, B. Eren, L. Moser, R. Steiner, E. Meyer, Can aluminium or magnesium be a surrogate for beryllium: a critical investigation of their chemistry, Fusion Eng. Des. 88 (2013) 1718–1721, https://doi.org/10.1016/j.fusengdes.2013.04.040.